An integrated model for dune morphology and sand fluxes on Mars

CrossMark

K.D. Runyon [a,*], N.T. Bridges [b,a], F. Ayoub [c], C.E. Newman [d], J.J. Quade [e]

[a] Johns Hopkins University, Department of Earth and Planetary Sciences, 301 Olin Hall, 3400 N. Charles Street, Baltimore, MD 21218, USA
[b] Johns Hopkins University, Applied Physics Laboratory, Planetary Exploration Group, 11101 Johns Hopkins Road, Laurel, MD 20723, USA
[c] Geological and Planetary Sciences, California Institute of Technology, MC 100-23, Pasadena, CA 91125, USA
[d] Aeolis Research, 600 N. Rosemead Blvd., Suite 205, Pasadena, CA 91107, USA
[e] University of Maryland, James A. Clark School of Engineering, 4611 College Ave, College Park, MD 20740, USA

ABSTRACT

The transport and deposition of sand is the most prevalent agent of landscape modification on Mars today, with fluxes comparable to some sand dunes on Earth. Until now, the relationship between sand flux and dune field morphology has been poorly constrained. By tracking dune movement over ~10 km-long dune fields in Herschel Crater and Nili Patera, representative of many dune fields on Mars, we find a downwind flux decrease that correlates with a sequence of changing morphology from barchans to barchanoids and seifs (longitudinal dunes) to isolated dome dunes and ending with sand sheets. We show empirical consistency with atmospheric Internal Boundary Layer (IBL) theory which can describe these broad flux and morphology changes in Martian dune fields. Deviations from IBL flux predictions are from wind streamline compressions up slopes, leading to a speedup effect. By establishing a dune field morphology type example and correlating it with measured and predicted flux changes, we provide an integrated morphology and flux model that can be applied to other areas of Mars and be used to infer paleo-environmental conditions from preserved sandstone.

© 2016 Elsevier B.V. All rights reserved.

1. Introduction

1.1. Martian aeolian environments

The Mariner 9 orbiter returned the first data indicating the presence of aeolian bedforms on Mars (Sagan et al., 1972). Sand dunes are now known to cover all major latitude zones (Hayward et al., 2007) and are common in craters, basins, the north polar region, and in the lee of topographic obstacles such as crater rims. With the exception of vegetated (e.g. parabolic) dunes, all of Earth's dune forms are represented on Mars: barchan, barchanoid, transverse, seif (or longitudinal), star, reversing, and dome. Mars' dunes are mobile and are not relics of past Martian climates (Silvestro et al., 2010; Bridges et al., 2012). In contrast to Earth, the aeolian processes responsible for dunes and other bedforms on Mars are unhindered by most other geomorphic agents, especially water. Indeed, on Mars the movement of sand and dust is the dominant process of geomorphic change in the current climate. The inferences gained from understanding regional and global sand transport pathways and erosional regimes provide constraints on current and past Martian climate (e.g. Grotzinger et al., 2005) and landscape evolution, in particular interpreting aeolian stratigraphy (Grotzinger et al., 2013; Milliken et al., 2014) and reconstructing paleoclimates, as has been done in terrestrial aeolian systems (Hunter, 1977; Clemmensen and Abrahamsen, 1983; Eastwood et al., 2012).

Given the need to understand modern dune patterns and sand flux variations, and to interpret paleoenvironments evidenced in sandstone stratigraphy, we establish links between modern sand fluxes, dune morphology sequences, dune height, and flux predictions from Global Circulation Models (GCMs). By combining the results of surface roughness changes and the GCM, we show consistency between measured and predicted fluxes for three sites. Two aeolian regions on Mars within the 300 km-diameter Herschel Crater (centered at 14°S, 130.1°E) and one region within the Nili Patera caldera (8.8°N, 67.3°E) serve as these case studies (Fig. 1), in which we used HiRISE (the High Resolution Imaging Science Experiment (McEwen et al., 2007)) images to measure dune height (from stereo digital elevation models), dune slip face advancement (Fig. S1), dune morphology (Fig. 2), ripple migration (Fig. 3), and dune volumetric crest flux across temporally-spaced images (see Text S1 in the Supporting Information).

The western and eastern Herschel Crater and the Nili Patera dune fields show similar dune morphological trends downwind in

---

* Corresponding author.
E-mail address: kirby.runyon@gmail.com (K.D. Runyon).
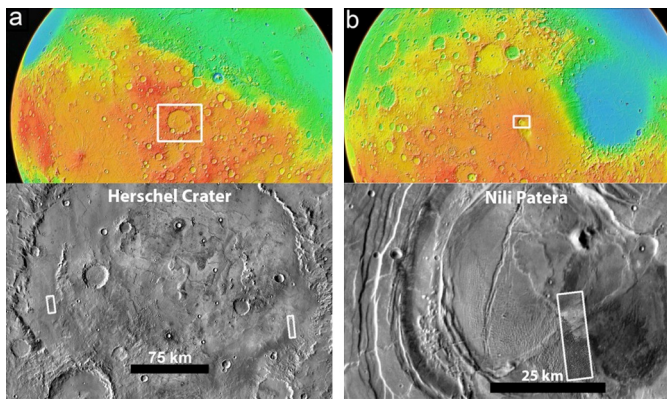
Fig. 1. An overview of the locations (white boxes, top) of (a) Herschel Crater and (b) Nili Patera. Western and eastern Herschel dune fields are boxed in the lower blow-up of Herschel (a), corresponding to available HiRISE coverage. Global views are MOLA colored topography from GoogleMars where warm colors indicate higher elevations than cooler colors. Regional images are HiRISE embedded in daytime THEMIS mosaics from JMARS (Christensen et al., 2009). North is up. (For interpretation of the references to color in this figure legend, the reader is referred to the web version of this article.)

which the dune morphologies transition from classical barchans to sand sheets (Fig. 2) and have been described by Cardinale et al. (2012, 2016). We identify this morphological trend as an illustrative type-example of dune field (Fig. 2). Importantly, their upwind margins are sharply defined and they all sit on bedrock as opposed to a sandy substrate.

Geomorphologically, some dunes exhibit asymmetry. Asymmetric barchans in western Herschel alternate between the west and east horns being longer whereas in eastern Herschel the west horns are more consistently longer. Dunes in Nili Patera, in contrast, are highly symmetric with relatively few dunes exhibiting horn asymmetry. Whereas our case study sites are constrained by the HiRISE footprints (necessary for temporal comparison of small scale features), broader Context Camera (CTX; (Malin et al., 2007)) images reveal the dune fields extending for many kilometers with the same broad morphological evolutionary sequence. Within this broader view provided by CTX, the long axes of barchans rotate a few degrees, suggesting a regionally varying resultant sand transport azimuth; this is substantiated by Cardinale et al.'s (2016) measurement of slip face directions.

1.2. Internal boundary layer theory applied to aeolian systems

Atmospheric and field studies on Earth show that flat-plate internal boundary layer (IBL) theory applied to the inland White Sands dune field accurately predicts the measured sand fluxes downwind and that this flux decrease corresponds to a spatially evolving dune morphology (Jerolmack et al., 2012; Anderson and Chemacki, 2014); this has also been applied to coastal aeolian systems (Rasmussen, 1989). Dunes acting as roughness elements to the oncoming wind reduce the wind's shear stress downwind, either from the initial upwind roughness transition (Jerolmack et al., 2012) or from the field-wide roughness (Pelletier, 2015). Either way, the heterogeneous dune roughness controls IBL flow, shear stress, and therefore sediment flux at White Sands (Pelletier, 2015).

An IBL forms when an increase in surface roughness, such as the wind transitioning from blowing over bedrock to dunes, acts as a momentum sink and greatly increases turbulence (Anderson and Chemacki, 2014). At least one manifestation of this turbulence is in the form of Kelvin–Helmholtz instability rollers which form behind upwind dunes and impinge upon downwind dunes (Anderson and Chemacki, 2014). Due to turbulence and drag, momentum retardation diffuses upward and advects downwind such that the IBL thickens downwind (McLean and Smith, 1986). The region within
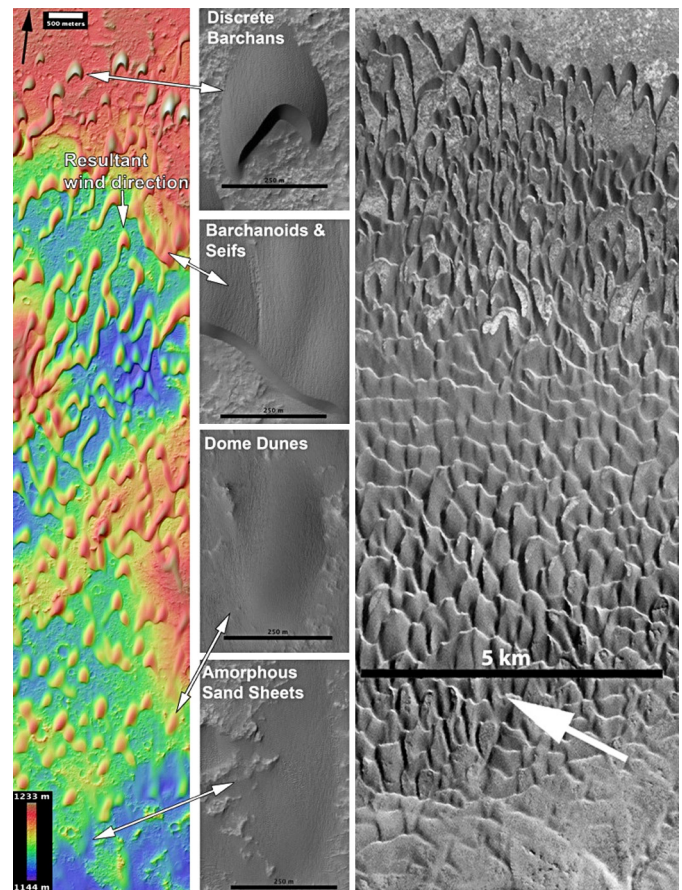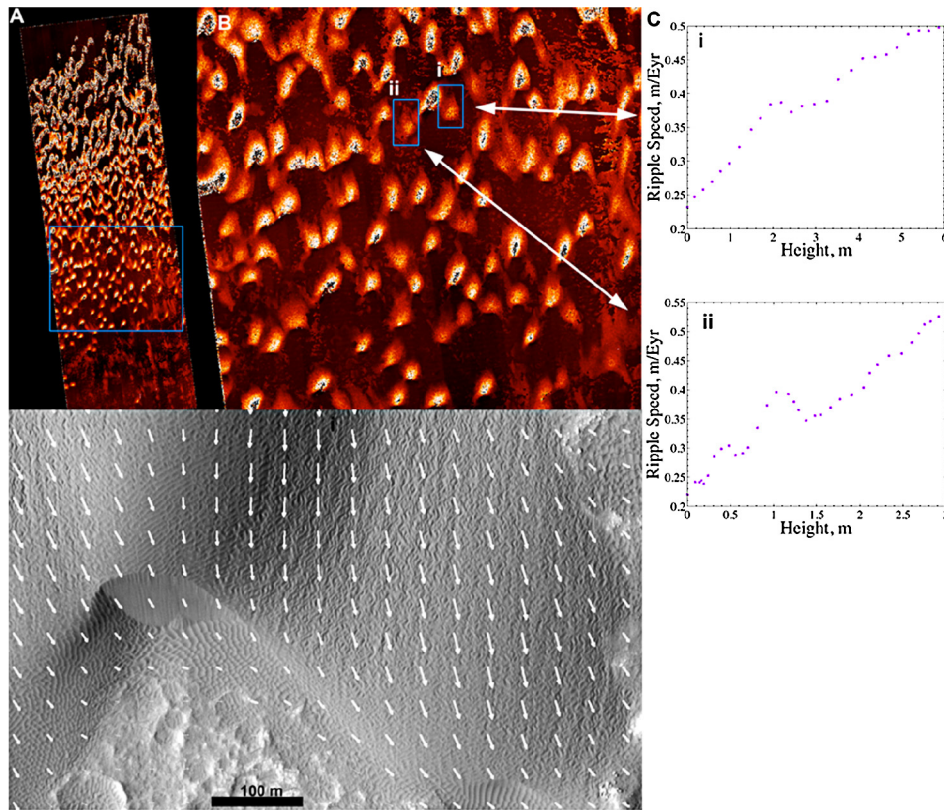

Fig. 2. The western Herschel Crater dune field (far left, height-colorized HiRISE DEM) and Nili Patera dune field (far right, CTX image) are type examples of a changing morphology downwind from barchan, to barchanoid and seif, to dome dunes, to sand sheets, each with successively lower heights and sand fluxes (north is indicated in each with a single-ended arrow; they have been rotated so that "downwind" is down). The term "downwind" is with regards to the apparent resultant transport direction evidenced by dune orientation. Less frequent but obliquely-blowing winds (up to angles >90°) likely produce asymmetrical dune elongation (Courrech du Pont et al., 2014), but obliquity effects are averaged over the several years between observations. The effect of obliquity on our IBL model may be to merely add a noise component. This morphology change is consistent with a decrease in downwind sand flux from the formation of an IBL, as observed at the White Sands dune field on Earth (Jerolmack et al., 2012). Note that the DEM is absolute elevation above Mars' datum. DEM credit: NASA/University of Arizona/USGS; HiRISE subscenes from PSP_002860_1650; CTX image B21_017762_1891_XN_09N292W, Credit: NASA/MSSS. (For interpretation of the references to color in this figure legend, the reader is referred to the web version of this article.)

the IBL is thus where the speed and shear stress are significantly different from upwind conditions (Garratt, 1990). The downwind thickening of the IBL occurs within the Atmospheric (or Planetary) Boundary Layer (ABL), which is a well-mixed turbulent layer of atmosphere between the Sun-heated ground and the stably stratified free atmosphere above. ABLs can be several km thick, and depending on the heat capacity of a planet's atmosphere may collapse (e.g. Savijarvi and Maattanen, 2010) to nearly zero height above the ground at night, as is often the case on Mars and is in accordance with our GCM.

Inspired by a similar geomorphological sequence observed at White Sands (Kocurek et al., 2010; Jerolmack et al., 2012) as in our Martian case study sites, we test the hypothesis that IBL theory can likewise describe the measured flux changes. Cardinale et al. (2016) hypothesized IBL-controlled sand fluxes for Herschel Crater dunes but did not test the hypothesis. Our work is the first time IBL theory has been quantitatively applied to Martian dune fields

Fig. 3. (A, B) A ripple displacement map of the western Herschel Crater dune field that has been covered by repeat HiRISE imagery. Brighter tones indicate greater ripple displacements (mostly north to south); speckled patterns indicate that ripples moved further than could be tracked by the COSI-Corr algorithm (see Methods). The HiRISE image is ~5 km across. (C) Ripple speeds (3.74 Earth years between images for western Herschel) increase up dunes' stoss slopes; this is likely from a wind speedup effect due to streamline compression up positive topography. Bridges et al. (2012) also found this to be the case on sand dunes in Nili Patera. (D) Ripple displacement vectors across dune (i) and its western companion dune. North is up.

and correlated with spatially evolving dune morphologies downwind.

In addition to applying the "Jerolmack IBL flux model" to our case study sites, we also model the pronounced effect of dune topography on wind speed and flux: Pelletier (2015) notes that topographic ridges within White Sands locally enhance shear stress and therefore sand flux from streamline compression. We therefore add the prediction that flux deviations from IBL theory ("noise") can be partly explained by wind streamline compressions from local slopes (Jackson and Hunt, 1975; Frank and Kocurek, 1996; Momiji et al., 2000; Gao et al., 2015) which operates as a secondary mechanism to the large-scale, dune field-wide IBL. The slope speedup occurs within a smaller, "nested" IBL on each dune (Frank and Kocurek, 1996).

IBL theory predicts average sand flux $\langle q_s \rangle$ as a function of distance downwind within an IBL as (Jerolmack et al., 2012)

$$\langle q_s \rangle = 0.055 I \frac{\rho_{\text{atmo}}}{\rho_{\text{solid}}} \frac{C}{g} \sqrt{\frac{D}{D_0}} U^3 \left(\frac{\nu}{U z_{0L}^{1/5}} \right)^{3/8} x^{-3/10} \quad (1)$$

where the ρ_{atmo} and ρ_{solid} are the atmospheric and grain densities, respectively; C is the aerodynamic drag coefficient; g is gravity; D is the characteristic sand grain size; D_0 is the standard reference grain size; U is the free stream air velocity at the top of the ABL, ν is the atmospheric kinematic viscosity; z_{0L} is the Lettau roughness height (Lettau, 1969); x is the distance downwind starting at the upwind tip of the dune field; and 0.055 is an empirical constant that is notably 10 times larger than the value used on Earth by Jerolmack et al. (2012) and its use is further justified in Text S3. This flux value is then multiplied by 3.154×10^7 s Earth-year^{-1} to give flux in units of m^3 m^{-1} Earth-year^{-1}. The variables are given

in Table S1 and the sediment mobility intermittency I is considered below (Text S4, Fig. S2, Table S2).

The sediment mobility intermittency I is the fraction of time that sediment is mobilized by the wind and is related to the time-averaged dune field flux $\langle q_s \rangle$ as (Jerolmack et al., 2012)

$$\langle q_s \rangle = I q_{\text{instantaneous}}.$$

The value Jerolmack et al. (2012) measured in situ at White Sands is $I = 0.03$, meaning that sediment moves 3% of the time.

The free stream velocity U associated with sand flux in Equation (1) is the unencumbered wind speed at the top of the ABL (the base of the stably-stratified free atmosphere) and is given by the law-of-the-wall

$$U = \frac{u_a^*}{\kappa} \ln \left(\frac{z}{z_{0L}} \right) \quad (2)$$

and is calculated from the average above-critical friction speed u_a^* from the GCM. The von Kármán constant $\kappa = 0.4$, z is ABL height, and z_{0L} is the Lettau roughness height (Lettau, 1969) (Text S4 and Tables S1–S2). Atmospheric densities ρ_{atmo} are Martian-yearly averages corresponding to above-critical shear stresses for the study sites ranging from 1.3–1.5×10^{-2} kg m^{-3} as output from the GCM. Terrestrial deserts have ABL heights 1–3 km above the ground (Lorenz and Zimbelman, 2014) whereas from our GCM, Mars ABL heights are ~9–11 km high. For our Herschel and Nili case study sites using $u_a^* \sim 1.1$ m s^{-1} from our GCM, the estimated free stream velocities 10 km high are ~24–27 m s^{-1}. This compares favorably with the terrestrial value
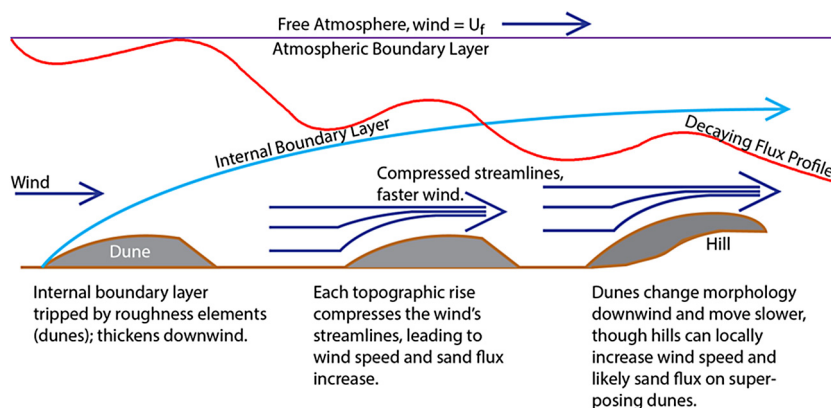
Fig. 4. Conceptual model illustrating IBL formation and topographic wind speedup effect as competing phenomena. The left-most upwind dune serves as a roughness element to trip an IBL which thickens downwind (toward the right). Each topographic rise (dune or bedrock) compresses the wind's streamlines, leading to wind speed, shear stress, and sand flux increase at a local scale; our use of the panel method does not consider the low slopes of the broad wavelength topography. The bulk motion of dunes slows and the dune morphology changes further afield as the IBL thickens. The wavy red curve illustrates the combined sand flux effects from the IBL and the streamline compression with an overall flux decrease that follows a power law but with dune-scale flux increases. (For interpretation of the references to color in this figure legend, the reader is referred to the web version of this article.)

of 20 m s^{-1} 1.9 km high for White Sands, NM (Jerolmack et al., 2012).

1.3. Slope speedup and the integrated model

Our accounting for topographic wind speedup has its precedent in field, laboratory, and theoretical studies: terrestrial anemometer measurements (McKenna Neuman et al., 1997) document accelerated wind speeds up reversing dune stoss slopes which agree with dune wind models (Momiji et al., 2000). On Mars, slope-induced streamline compression accounts for the observation that ripples accelerate upslope (Bridges et al., 2012). Several authors have discussed speedup ratios or speedup factors for wind blowing over hills and bedforms (e.g. Jackson and Hunt, 1975; Momiji et al., 2000; Gao et al., 2015; Pelletier, 2009; Lancaster, 1985), and Pelletier (2015) discusses the importance of wind flow line convergence (i.e., streamline compression) up slopes and the resulting increase in wind shear stress. Modeling wind speedups from topographic slopes goes back to at least the 1970s with civil engineering applications in mind (Jackson and Hunt, 1975), though not all authors relate wind speedups with explaining increases in sand flux; authors that do include, e.g. McKenna Neuman et al. (1997), Wiggs et al. (1996), Pelletier (2015), Momiji et al. (2000), and Bourke et al. (2004). Given the higher shear stress and sand mobilization potential of topographically-accelerated wind, we consider a wind speedup factor in which 1 indicates no speedup, larger than 1 indicates speedup, and factors 0–1 indicate slowdown, such as for streamline divergence in the lee of topography (Lancaster, 1985). We use the speedup factor to modify U used in the IBL flux prediction (Equation (1)) along a topographic transect and thus add to the Jerolmack IBL flux model to better explain the scatter in flux data.

Fig. 4 illustrates our model conceptually for dune flux evolution and describes the downwind morphological evolution in sand dunes and changes in crest flux by invoking an IBL modified by both bedrock and dune topography. The downwind-thickening IBL lowers flux, resulting in progressively smaller dunes downwind that eventually lack slip faces, which give way to sand sheets. Dunes perched on positive topography may experience higher sand fluxes because the streamline compression partially offsets decreases in wind speed. However, at sufficient height, the dunes should erode due to higher wind shear stresses which prevent deposition; this acts to limit dune height growth (e.g. Kok et al., 2012).

2. Methods

2.1. Measuring topography and bedform displacement

The HiRISE camera, orbiting Mars on the Mars Reconnaissance Orbiter (MRO), provides ground imagery of ∼0.25 m/px and derived Digital Elevation Maps (DEMs) with post spacings of 1 m/px and 10s of cm of vertical precision, processed from stereo pairs (Kirk et al., 2008). We re-projected HiRISE images onto stereo HiRISE-derived DEMs to create orthoimages, thus allowing for subpixel co-registration of images separated in time using the ENVI plug-in Co-registration of Optically Sensed Images and Correlation (COSI-Corr) (Leprince et al., 2007). Thus, we used three HiRISE images per area for a total of nine HiRISE images for this study: two images to build a DEM and the first and third images for both manual change detection of slip faces and automatic change detection of ripple patterns using COSI-Corr in the manner of Bridges et al. (2012). We mapped the location of barchan dune slip faces along a downwind transect in both time-separated images (Fig. S1) and divided the area of slip face advancement by the arc length of the active slip face, arriving at a characteristic displacement for a particular dune. Dividing by the time interval between images gives bulk dune speed; multiplying by dune crest height as measured from the DEM yielded dune crest flux.

2.2. Global circulation model and grain mobility intermittency

In lieu of in situ wind speed measurements that are lacking at the Martian sites, we used a 2-degree resolution GCM to produce atmospheric predictions for our case study in Nili Patera and a 0.074-degree resolution nested mesoscale domain inside the GCM for our studies in Herschel Crater. At each grid point, the predicted friction speed u^* and near-surface air density ρ_a were output every three Mars hours (1 Mars hour = 1/24 of a sol) for one Mars year. The output from all grid points in each study region was then used to produce a combined wind shear stress histogram (1000 bins) for that region, where wind shear stress $\tau = \rho u^{*2}$. We used an effective critical shear stress τ_c of 0.01 ± 0.015 N m^{-2} which parameterizes both the initiation and continuation of basaltic sand grain movement ($\rho_{basalt} = 2850$ kg m^{-3}). This value of τ_c resulted in the best match between the seasonality of observed sand fluxes in Nili Patera and those predicted by the same GCM used in this study (Ayoub et al., 2014). I is derived from integrating and ratioing the wind shear stress histogram for all shear stresses and

those only at and above threshold, thereby yielding the fractional time that wind is above τ_c. (We describe the detailed computation of I in Text S2, Fig. S2, and Table S2.) The intermittency values are lower bounds since the wind stresses predicted by the GCM do not account for mesoscale and higher resolution effects such as local turbulent lee eddies (Anderson and Chemacki, 2014; Palmer et al., 2012) and small-scale slope-induced wind speed changes; this may be a source of flux under-prediction. For western and eastern Herschel and Nili Patera, the average computed intermittency values are ∼0.8%, 2.5%, and 9.2%, respectively, assuming a mean critical threshold shear stress of $\tau_c = 0.01 \text{ N m}^{-2}$. These values for I compare with 3% (0.03) measured at White Sands (Jerolmack et al., 2012). We also used $u*$ from the GCM to calculate the free stream velocity, U at the top of the ABL (Equation (2)) and the predicted IBL-controlled flux (Equation (1)).

2.3. Wind speedup from the panel method

Whereas much work (e.g. Anderson and Chemacki, 2014; McLean and Smith, 1986; Palmer et al., 2012) was focused on wind speed and turbulence effects from dune topography, many of these studies did not make the less-clear link from wind speed to sand flux. To calculate the amount of wind speed increase, we assume incompressible and inviscid air flow, topographic rise ("bump") symmetry, and discretize the bumps into "panels." Each bump is regarded as a symmetric isosceles triangle. Even though topographic features are not necessarily symmetric, the symmetry assumption is still valid: leeward eddies act as part of the bump to the wind passing overhead, rendering the effective bump essentially symmetric. This simple panel method (Hess, 1990) serves as an approximation to Laplace's equation and is a common approach to solving simple problems in incompressible and inviscid fluid flow around subsonic aircraft, and we justify its debut in aeolian geology from its successful application in aeronautical engineering. We calculate a parameter λ as

$$\lambda = \frac{6\pi \sin(\theta)}{-2\sqrt{3}\sin(\theta) + 3\cos(\theta) + 3\pi} \tag{3}$$

where θ is the smoothed slope at each adjacent post spacing in our DEM. We then use λ to calculate the wind speedup factor, u_{inc}

$$u_{inc} = 1 + 2\left(\frac{\lambda \cos(\theta)}{\pi} + \frac{\lambda \cos(2\theta)}{\pi\sqrt{3}}\right). \tag{4}$$

We calculated the slope from a downwind-trending topographic profile from a smoothed 1-m post-spacing DEM and used the slope at every DEM post (1 m spacing) to determine the topographic wind speedup. The wind speed solution to the panel method at every point was then used for the wind speed U of equation (1) to calculate estimated flux profiles downwind in three areas of our case study. The speedup factor is only dependent on the slope of the bump, not its physical size, in part because the wind flow is fully turbulent at all length scales (Kok et al., 2012). Typical wind speedup factors of between 1 and 1.15 are common, where a factor of 1 means no speedup. For example, the panel method predicts a wind velocity increase of factor 1.05 for a 2° slope. Appropriately, the panel method predicts a wind decrease for negative slopes.

The panel method gives speedup factors notably lower than the values of ∼1.5–3 measured in the field (McKenna-Neumann et al., 1997; Lancaster, 1985) and also only considers the slope of topography, not its physical size. Justifying our use of it and accepting its lower speedup factors is that McKenna-Neumann et al. (1997) measured speedup on steep reversing dunes with slopes up to 14.5°; 5° is a common stoss angle for downwind western Herschel Crater barchan and dome dunes. Furthermore, when we use the panel method's speedup factors in the Jerolmack et al. (2012)

flux equation, the flux predictions match the data. When we used higher speedup factors the predictions were at least an order of magnitude larger than the flux data.

The IBL flux equation (Equation (1)) provides a baseline annual-average flux. In some sense, it assumes the dunes are flat, two-dimensional structures on the ground insofar as there is no topography term in the equation. The flux increase from the streamline compression up the dunes' stoss slopes is therefore superimposed on the baseline flux. As such, the slope speedup does not affect the field scale IBL but only affects local flux deviations from the IBL flux predictions.

## 3. Results

3.1. Measured dune heights and fluxes

Measured dune crest fluxes for the three case studies are in Fig. 5. Dune heights for both Herschel areas are in Fig. 6.

Numerical values for the following are an average for both Herschel sites but the qualitative concept applies to Nili and elsewhere. Beginning in the upwind margin, the aeolian fields are composed of well-developed, discrete barchan dunes that are on average ∼17–22 m high at their crest with ∼5–15 $\text{m}^3 \text{m}^{-1} \text{yr}^{-1}$ of sand flux (Fig. 5), the same as White Sands (Jerolmack et al., 2012), with an estimated flux measurement uncertainty of ∼10% (Fig. S1). Well-exposed bedrock crops out between dunes. Midfield (1–4 km downwind), the dunes overlap, forming barchanoids with well-developed slip faces, and seif dunes. Many barchan horns become elongated, forming incipient seif dunes attached to asymmetric barchans and on the whole, dunes interact via merging, lateral linking, calving, and off-center collisions, thereby evolving the dune field pattern (Kocurek et al., 2010). Still further downwind (6–8 km from the upwind margin), the dunes are again separate and discrete from each other, though they are shorter (∼10 m at their crests) than the most upwind dunes, and many are dome dunes which lack slip faces. Measured crest fluxes on the small barchans with slip faces are ∼1–3 $\text{m}^3 \text{m}^{-1} \text{yr}^{-1}$. Furthest downwind (8–11 km), sand sheets cover the bedrock. All dunes are separated from their nearest upwind dune from zero to a few hundred meters with only a slight increase in dune spacing downwind. The morphology transitions cannot be uniquely tied to specific sand flux values and their associated transition distances are even more varied elsewhere.

3.2. Model flux predictions

Herschel dunes form larger roughness elements than the locally rough bedrock geology (Fig. S3). Defining roughness as the standard deviation of the height of an area (Jerolmack et al., 2012), the dunes are several (2–5) times rougher than the upwind bedrock for the western Herschel dune field, which we model as tripping the IBL. The flux data are consistent with a power-law decrease in volumetric sand flux, and this is also predicted from Equation (1). This is – overall – consistent with the formation of an IBL (Fig. 5) which predicts a flux decrease with power law slope = −0.3. High-frequency deviations from the IBL flux prediction from local topography likely cause some of the scatter in the flux profile measurements and are of the same magnitude as deviations in the flux measurements. These curves are for different values of I based on the ±0.0015 N m^{-2} (15%) uncertainty in $\tau_c = 0.01$ N m^{-2} (Ayoub et al., 2014). The right-hand panels in Fig. 5 show topography and slope used to calculate wind speedup effects along ∼300–500 m-wide transects down the dune fields, which average topographies width-wise. A given dune may not necessarily lie along the representative topographic transects, thus a one-to-one correspondence between a power law flux deviation (i.e., a slope speedup) and a given crest-flux data point is not expected.
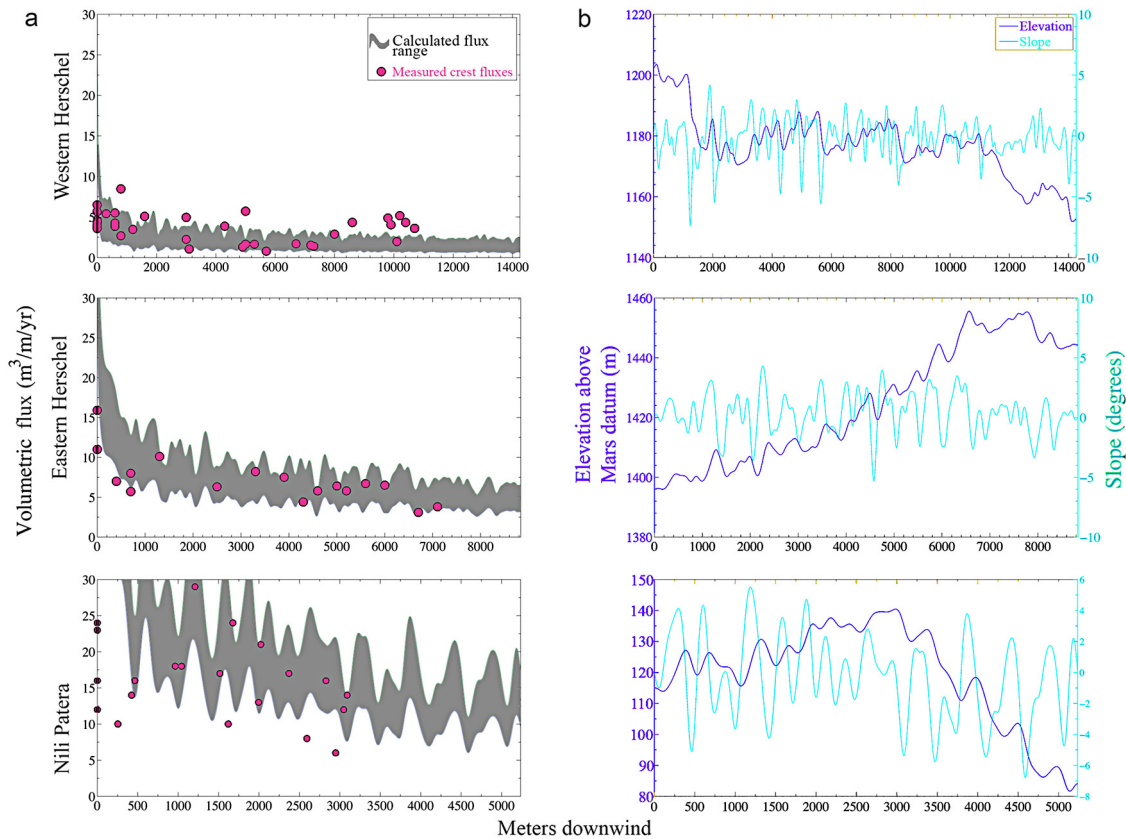
Fig. 5. Trends in crest flux (in m³ m⁻¹ Earth-year⁻¹) (a), elevation, and slope (b) as a function of distance downwind from the upwind dune margin for western and eastern Herschel and Nili Patera. (a) The gray curves show flux predictions for different values of intermittency corresponding to uncertainty in critical shear stress (given in the text). Lower flux predictions correspond to higher-strength but more rare winds. Pink circles are measured volumetric crest flux measurements per sand dune. The data are enveloped by the range of a priori power law flux decay predictions. (b) Elevation (height above Mars datum) shown in purple on the left axis and the slope (derivative of elevation) shown in cyan (right axis). Each topographic transect was several hundred pixels wide to average width-wise over topography; it was subsequently smoothed over a few meters length-wise to minimize effects of very short wavelength topography or artifacts in the DEM. We only applied the panel method to adjacent DEM posts and so it is not sensitive to long wavelength topography. Note a strong correspondence between the slope and the slope-induced flux prediction. Panel method predictions of flux increase are of the same magnitude as scatter in the data and are superimposed as perturbations on the IBL flux decay curve. (For interpretation of the references to color in this figure legend, the reader is referred to the web version of this article.)
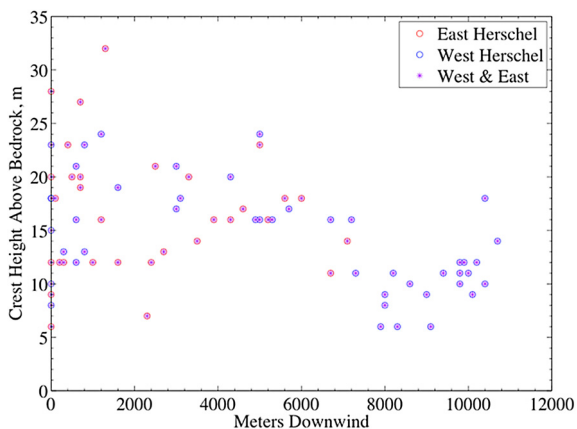
Fig. 6. Dune heights measured from stereo HiRISE-derived DEMs plotted as a function of distance downwind for both western and eastern Herschel dune fields.

4. Discussion

4.1. Justification for invoking IBL theory

Bolstering the applicability of the Jerolmack flux equation (Equation (1)) and thus the IBL interpretation of flux is that the model is agnostic regarding measured flux data and yet fits the overall measured flux values and their decay downwind, both on the Martian case study sites and at Earth's White Sands (Jerolmack et al., 2012). IBLs are not the only way to explain lessening sand flux downwind, however. The decrease in sand flux downwind could be partly attributed to "substrate sequestration" of sand by deposition in interdune areas, which removes sand from the dynamic system. However, this effect is likely very minimal, as we observe the dunes to sit directly on bedrock. They are not perched on a substrate of sand as is the case with White Sands (Langford, 2003 and the references therein).

Pelletier's (2015) model may partly apply to the Martian dune field case studies. The principle difference between the Pelletier and Jerolmack et al. (2012) models is that Pelletier considers a dune field's overall topographic heterogeneity, not just the roughness transition at the upwind margin. However, whereas Jerolmack et al. (2012) explicitly mention the discrete roughness change upwind, their flux equation (our Equation (1)) considers just the dune field roughness, not the transition from upwind roughness. Like us, Pelletier (2015) considers as important the convergence of wind streamlines for enhancing shear stress and sand flux, which is mentioned but not mathematically accounted for by Jerolmack et al. (2012). In our study, we account for streamline compression by applying the panel method to topography from both bedrock and bedforms. A component of Pelletier's (2015) model that is almost certainly not applicable on present-day Mars is the dryness versus dampness of bedform sands; Mars' active

aeolian sands are undoubtedly dry. Our integrated model reasonably accounts for the observed spatial flux changes and combines the IBL-inducing roughness of the dune field (not undermined by Pelletier's analysis) and the streamline compressing attributes of Pelletier (2015).

4.2. Limitations and uncertainties

Our model ignores the initiation and cessation of saltation. Because wind speed correlates with slope, there are times when the top parts of dunes are actively saltating and the lower reaches are not. This could result in over-prediction of the amount of dune crest flux because our models assume that threshold friction speeds are met simultaneously for all parts of a stoss slope.

The R^2 fits between flux data points and IBL-only flux predictions are low (0.18, 0.64, and 0.04 for western and eastern Herschel and Nili, respectively). However, this is expected because of scatter from slope speedup, turbulence, and other effects.

Another limitation of our model is that it does not account for variations in sand flux azimuth suggested by barchan horn asymmetry (Fig. 7), some corrugated slip faces, and some incipient seif dunes. However, it is not clear that this makes a major effect on our model: Lv et al. (2016) showed that barchan asymmetry alone cannot be used to constrain the direction of a secondary wind. Parteli et al. (2014) describes several processes in addition to secondary winds which can cause dune asymmetry: ground slope, bedrock topography, and sediment flux direction, which are likely convolved in our case study sites. Regarding secondary flows which may be present in our study sites, Parteli et al. (2014) model that elongated barchan horns can become seif dunes and Courrech du Pont et al. (2014) demonstrate the elongating "fingering" of longitudinal and oblique dunes. Dune collisions seem to be prevalent, partly as evidenced from "stacked" slip faces. Our IBL-plus-slope speedup flux model is ideally suited for unidirectional transport azimuths (e.g. winds), yet still seems applicable with azimuthally varying sand transport (e.g. Courrech du Pont et al., 2014), as long as one azimuth dominates, e.g., with a primary-to-secondary transport ratio of ∼five (Courrech du Pont et al., 2014). Our model is not applicable when more than one transport direction dominates (e.g., a lower transport ratio) or where the topography is extreme (near the repose angle) and gravity begins to dominate over wind, e.g., in Valles Marineris (Chojnacki et al., 2014).

The lack of correlation between dune morphology and sand fluxes in different dune fields should not be a problem for our model. More factors besides downwind flux decreases and upslope flux increases control dune morphology. These other issues may include sand availability, bedrock characteristics, sand transport azimuth, transport ratios (Courrech du Pont et al., 2014), and dune collisions (Kocurek et al., 2010) (which in turn depend on the other listed items). The main point of our model remains that IBL theory and slope speedup can explain flux changes downwind in dune fields with similar boundary conditions as Herschel and Nili (i.e., a Herschel-type dune field).

Finally, slope speedup effects from the panel method underpredict wind slope speedup compared with field measurements; however, when we used field-based wind speedup factors of 2–3 (McKenna Neuman et al., 1997), the predicted sand flux values were far above anything we measured from the slip faces. As in the case of Jerolmack et al. (2012), we ignored processes such as smaller-scale "nested" boundary layers (e.g. the "equilibrium layer" (Garratt, 1990)) (Frank and Kocurek, 1996), large and small scale eddies, flow re-attachment, and viscosity. We submit that these complications are implicitly parameterized in IBL theory and panel method slope speedup.
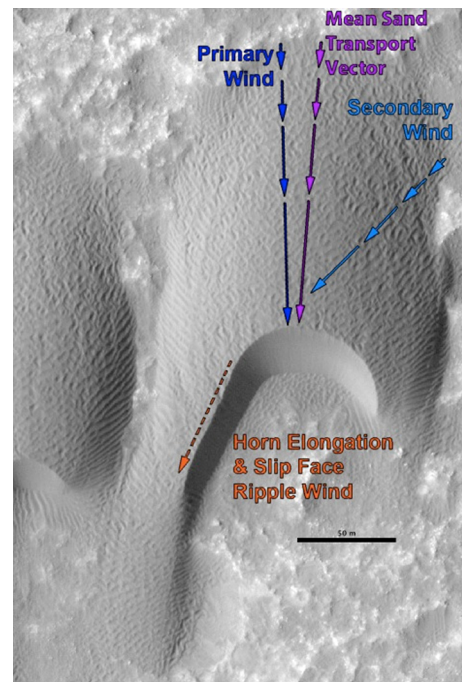

Fig. 7. A western Herschel asymmetric barchan dune with arrows schematically illustrating primary (left, blue), secondary (right, cyan), and resultant (purple, center) wind directions. The secondary wind can elongate one of the barchan horns (left, orange) and also add corrugated ripples to part of the slip face. The three arrows on the dune's stoss side also schematically illustrate the stoss slope speedup effect via ever-lengthening arrows. HiRISE image PSP_002860_1650; north is up. (For interpretation of the references to color in this figure legend, the reader is referred to the web version of this article.)

5. Implications

5.1. Dunes as geologic systems on Mars

Our proposed flux model should have widespread applicability where IBL development controls the flow of wind and where other factors, such as topography or sediment supply, do not dominate. Naturally, this model is not applicable to, for instance, falling dunes in Valles Marineris (Chojnacki et al., 2014) or dunes with reversing slip faces, indicative of widely varying wind azimuths. But, for the many barchan dune fields on Mars, Earth, and perhaps Titan and Venus (which await reconnaissance at higher resolution), the tenants of our model will provide useful and insightful sand flux estimations, especially when temporal image coverage or in situ sand volume measurements of a region are lacking.

5.2. Martian aeolian stratigraphic record

Understanding current aeolian environments aids interpretation of lithified aeolian sediment, and the ongoing exploration of Mars is providing more instances of aeolian stratigraphy (e.g. Grotzinger et al., 2005; Milliken et al., 2014; Lapotre et al., 2016). For example, Lapotre et al. (2016) demonstrate that new insights into Martian aeolian bedform dynamics can aid in the interpretation of sandstone records of paleo-environments. In their paper, Lapotre et al. (2016) re-interpret ripples seen in HiRISE images as subaerial fluid-drag ripples, analogous to subaqueous ripples on Earth, both of which are strongly influenced by the fluids' viscosity. They then identify these ripples preserved in exposed sandstone cliffs at Victoria Crater as imaged from the rover *Opportunity* and interpret the late-Noachian depositional paleo-environment as one with a thin, viscous atmosphere. More related to sand flux, in Gale Crater's sandstone deposits the rover *Curiosity* imaged foreset beds,

cross stratification, and truncated erosional surfaces, interpreted as aeolian in origin (Grotzinger et al., 2015). Similarly, Milliken et al. (2014) provide evidence that dunes may lithify and remain identifiable in both planform and eroded cross section from orbital imagery. In such cases the slip face and crest orientations remain identifiable, likewise indicating a paleo-aeolian environment in a region that may no longer be dominated by sand flux. Future surface exploration of Mars will undoubtedly discover more lithified aeolian sandstone in outcrop. Where preserved in the Martian sandstone stratigraphic record, our documented morphologic evolution can be recorded as transitions from dunes with slip faces (preserved as foreset beds) to bedforms lacking slip faces (climbing and falling cross stratification), as well as grain size transitions from coarse to fine downwind (Jerolmack et al., 2011).

With a downwind decaying sand flux for our Martian case studies and the White Sands case study (Jerolmack et al., 2012; Pelletier, 2015), one would predict net accumulation due to the ever-weakening downwind flux. Rather, we see sand dunes transition to sand sheets, which thin before disappearing downwind in the case of the Herschel aeolian fields or abutting bedrock in the case of Nili's dune field. Reconciling the disparate prediction and observation is difficult. Perhaps the dune fields are quite young (few 10s kyr) and have not had time to accumulate an immobile sand layer atop the bedrock. To illustrate the potential youth of dune fields, it would take only 40 kyr for an upwind dune moving a typical speed of 0.25 m Earth-year^{-1} to reach the downwind margin 10 km away and given enough time, accumulation of aeolian strata will occur. Or, perhaps the maximum wind shear stress never falls below the fluid threshold and the entire dune and sand sheet field migrates downwind with a constant sand supply and no net accumulation ever occurs. Further research into Martian sediment pathways, bedform dynamics, and climate cycles may elucidate this mystery (e.g. Chojnacki et al., 2014; Lapotre et al., 2016).

6. Conclusions

We identify an aeolian dune morphological sequence as a type example on Mars with a downwind decreasing sand flux as consistent with the predictions from internal boundary layer theory and wind-slope speedup effects. The spatially-evolving sequence (the "Herschel-type dune field") begins upwind with barchan sand dunes and proceeds downwind with barchanoid and seif, dome dunes, and finally, sand sheets, which we find across Mars. We also demonstrate a novel method to quantitatively estimate sand flux intermittency I by integrating wind speed histograms from GCMs. Our sand flux measurements and morphological classifications from the Herschel Crater and Nili Patera dune fields are applicable to other sand dune fields on any planetary body exhibiting Herschel-type dune field characteristics. Our model appears to accurately predict flux trends regardless if the Jerolmack et al. (2012) or the Pelletier (2015) roughness assumptions are made. Thus we offer the IBL-plus-slope speedup integrated model as a convenient semi-empirical model for predicting sand flux within Herschel-type dune fields on Mars, Earth, Venus, and Titan without the need for temporal image coverage.

Acknowledgements

Appendix A. Supplementary material

Supplementary material related to this article can be found online at http://dx.doi.org/10.1016/j.epsl.2016.09.054.

References

Anderson, W., Chemacki, M., 2014. Numerical study of turbulent flow over complex aeolian dune fields: the White Sands National Monument. Phys. Rev. E 89. http://dx.doi.org/10.1103/PhysRevE.89.013005.

Ayoub, F., et al., 2014. Threshold for sand mobility on Mars calibrated from season variations of sand flux. Nat. Commun. 6096, 1–8. http://dx.doi.org/10.1038/ncomms6096.

Bourke, M.C., Bullard, J.E., Barnouin-Jha, O.S., 2004. Aeolian sediment transport pathways and aerodynamics at troughs on Mars. J. Geophys. Res. 109, E07005. http://dx.doi.org/10.1029/2003JE002155.

Bridges, N.T., et al., 2012. Earth-like sand fluxes on Mars. Nature 485, 339. http://dx.doi.org/10.1038/nature11022.

Cardinale, M., et al., 2016. Present-day aeolian activity in Herschel Crater, Mars. Icarus 265, 139–148. http://dx.doi.org/10.1016/j.icarus.2015.10.022.

Cardinale, M., Komatsu, G., Silvestro, S., Tirsch, D., 2012. The influence of local topography for wind direction on Mars: two examples of dune fields in crater basins. Earth Surf. Process. Landf. 37, 1437–1443. http://dx.doi.org/10.1002/esp.3289.

Chojnacki, M., Burr, D.M., Moersch, J.E., Wray, J.J., 2014. Valles Marineris dune sediment provenance and pathways. Icarus 232, 187–219. http://dx.doi.org/10.1016/j.icarus.2014.01.011.

Christensen, P.R.E., et al., 2009. JMARS – a planetary GIS. http://adsabs.harvard.edu/abs/2009AGUFMIN22A..06C.

Clemmensen, L.B., Abrahamsen, K., 1983. Aeolian stratification and facies association in desert sediments, Arran basin (Permian), Scotland. Sedimentology 30, 311–339. http://dx.doi.org/10.1111/j.1365-3091.1983.tb00676.x.

Courrech du Pont, S., Narteau, C., Gao, X., 2014. Two modes for dune orientation. Geology 42 (9), 743–746. http://dx.doi.org/10.1130/G35657.1.

Eastwood, E.N., et al., 2012. Methodology for reconstructing wind direction, wind speed and dune events from aeolian cross-strata. J. Geophys. Res. 117, F03035. http://dx.doi.org/10.1029/2012JF002368.

Frank, A.J., Kocurek, G., 1996. Airflow up the stoss slope of sand dunes: limitations of current understanding. Geomorphology 17, 47–54. http://dx.doi.org/10.1016/0169-555X(95)00094-L.

Gao, X., Narteau, C., Rozier, O., 2015. Development and steady state of transverse dunes: a numerical analysis of dune pattern coarsening and giant dunes. J. Geophys. Res., Earth Surf. 120, 2200–2219. http://dx.doi.org/10.1002/2015JF003549.

Garratt, J.R., 1990. The internal boundary layer – a review. Bound.-Layer Meteorol. 50, 171–203.

Grotzinger, J.P., et al., 2005. Stratigraphy and sedimentology of a dry to wet eolian depositional system, Burns formation, Meridiani Planum, Mars. Earth Planet. Sci. Lett. 240, 11–72. http://dx.doi.org/10.1016/j.epsl.2005.09.039.

Grotzinger, J.P., et al., 2013. A habitable fluvio-lacustrine environment at Yellowknife Bay, Gale Crater, Mars. Science 343, 1242777. http://dx.doi.org/10.1126/science.1242777.

Grotzinger, J.P., et al., 2015. Deposition, exhumation, and paleoclimate of an ancient lake deposit, Gale crater, Mars. Science 350, 6257. http://dx.doi.org/10.1126/science.aac7575.

Hayward, R.K., et al., 2007. Mars global digital dune database and initial science results. J. Geophys. Res. 112, E11007. http://dx.doi.org/10.1029/2007JE002943.

Hess, J.L., 1990. Panel methods in computational fluid dynamics. Annu. Rev. Fluid Mech. 22, 255–274.

Hunter, R., 1977. Basic types of stratification in small aeolian dunes. Sedimentology 24, 361–387. http://dx.doi.org/10.1111/j.1365-3091.1977.tb00128.x.

Jackson, P.S., Hunt, J.C.R., 1975. Turbulent wind flow over a low hill. Q. J. R. Meteorol. Soc. 101, 929–955. http://dx.doi.org/10.1002/qj.49710143015.

Jerolmack, D.J., Reitz, M.D., Martin, R.L., 2011. Sorting out abrasion in a gypsum dune field. J. Geophys. Res. 116, F02003. http://dx.doi.org/10.1029/2010JF001821.

Jerolmack, D.J., et al., 2012. Internal boundary layer model for the evolution of desert dune fields. Nat. Geosci. 5, 206–209. http://dx.doi.org/10.1038/ngeo1381.

Kirk, R.L., et al., 2008. Ultrahigh resolution topographic mapping of Mars with MRO HiRISE stereo images: meter-scale slopes of candidate Phoenix landing sites. J. Geophys. Res., Planets 113, E3. http://dx.doi.org/10.1029/2007JE003000.

Kocurek, G., Ewing, R.C., Mohrig, D., 2010. How do bedform patterns arise? New views on the role of bedform interactions within a set of boundary conditions. Earth Surf. Process. Landf. 35, 51–63. http://dx.doi.org/10.1002/esp.1913.

Kok, J.F., et al., 2012. The physics of wind-blown sand and dust. Rep. Prog. Phys. 75. http://dx.doi.org/10.1088/0034-4885/75/10/106901.

Lancaster, N., 1985. Variations in wind velocity and sand transport on the windward flanks of desert sand dunes. Sedimentology 32, 581–593. http://dx.doi.org/10.1111/j.1365-3091.1985.tb00472.x.

Langford, R.P., 2003. The Holocene history of the White Sands dune field and influences on eolian deflation and playa lakes. Quat. Int. 104, 31–39. http://dx.doi.org/10.1016/S1040-6182(02)00133-7.

Lapotre, M.G.A., et al., 2016. Large wind ripples on Mars: a record of atmospheric evolution. Science 353, 6294. http://dx.doi.org/10.1126/science.aaf3206.

Leprince, S., et al., 2007. Automatic and precise orthorectification, coregistration, and subpixel correlation of satellite images, application to ground deformation measurements. IEEE Trans. Geosci. Remote Sens. 45, 1529–1558. http://dx.doi.org/10.1109/TGRS.2006.888937.

Lettau, H., 1969. Note on Aerodynamic Roughness-Parameter Estimation on the Basis of Roughness-Element Description. Research & Development technical report ECOM 66-G24-F. http://dx.doi.org/10.1175/1520-0450(1969)008<0828:NOARPE>2.0.CO;2.

Lorenz, R.D., Zimbelman, J.R., 2014. Dune Worlds: How Windblown Sand Shapes Planetary Landscapes. Springer.

Lv, P., Dong, Z., Narteau, C., Rozier, O., 2016. Morphodynamic mechanisms for the formation of asymmetric barchans: improvement of the Bagnold and Tsoar models. Environ. Earth Sci. 75, 259. http://dx.doi.org/10.1007/s12665-015-5083-2.

Malin, M.C., et al., 2007. Context camera investigation on board the Mars Reconnaissance Orbiter. J. Geophys. Res., Planets 112 (E5). http://dx.doi.org/10.1029/2006JE002808.

McEwen, S., et al., 2007. Mars Reconnaissance Orbiter's High Resolution Imagine Science Experiment (HiRISE). J. Geophys. Res. 112 (E5). http://dx.doi.org/10.1029/2005JE002605.

McKenna Neuman, C., Lancaster, N., Nickling, W.G., 1997. Relations between dune morphology, air flow, and sediment flux on reversing dunes, Silver Peak, Nevada. Sedimentology 44. http://dx.doi.org/10.1046/j.1365-3091.1997.d01-61.x.

McLean, S.R., Smith, J.D., 1986. A model for flow over two-dimensional bedforms. J. Hydraul. Eng. 112 (4), 300–317. http://dx.doi.org/10.1061/(ASCE)0733-9429(1986)112:4(300).

Milliken, R.E., Ewing, R.C., Fisher, W.W., Hurowitz, J., 2014. Wind-blown sandstones cemented by sulfate and clay minerals in Gale Crater, Mars. Geophys. Res. Lett. 41, 1149–1154. http://dx.doi.org/10.1002/2013GL059097.

Momiji, H., Carretero-González, R., Bishop, S.R., Warren, A., 2000. Simulation of the effect of wind speedup in the formation of transverse dune fields. Earth Surf. Process. Landf. 25, 905–918.

Palmer, J.A., Mejia-Alvarez, R., Best, J.L., Christensen, K.T., 2012. Particle-image velocimetry measurements of flow over interacting barchan dunes. Exp. Fluids 52, 809–829. http://dx.doi.org/10.1007/s00348-011-1104-4.

Parteli, E.J.R., et al., 2014. Origins of barchan dune asymmetry: insights from numerical simulations. Aeolian Res. 12, 121–133. http://dx.doi.org/10.1016/j.aeolia.2013.12.002.

Pelletier, J.D., 2009. Controls on the height and spacing of eolian ripples and transverse dunes: a numerical modeling investigation. Geomorphology 105. http://dx.doi.org/10.1016/j.geomorph.2008.10.010.

Pelletier, J.D., 2015. Controls on the large-scale spatial variations of dune field properties in the barchanoid portion of White Sands dune field, New Mexico. J. Geophys. Res., Earth Surf. 120, 453–473. http://dx.doi.org/10.1002/2014JF003314.

Rasmussen, K.R., 1989. Some aspects of flow over coastal dunes. Proc. R. Soc. Edinb., Sect. B 96, 129–147. http://dx.doi.org/10.1017/S0269727000010897.

Sagan, C., et al., 1972. Variable features on Mars: preliminary Mariner 9 television results. Icarus 17, 346–372. http://dx.doi.org/10.1016/0019-1035(72)90005-X.

Savijarvi, H., Maattanen, A., 2010. Boundary-layer simulations for the Mars Phoenix lander site. Q. J. R. Meteorol. Soc. 136, 1497–1505. http://dx.doi.org/10.1002/qj.650.

Silvestro, S., Fenton, L.K., Vaz, D.A., Bridges, N.T., Ori, G.G., 2010. Ripple migration and dune activity on Mars: evidence for dynamic wind processes. Geophys. Res. Lett. 37, L20203. http://dx.doi.org/10.1029/2010GL044743.

Wiggs, G.F.S., Livingstone, I., Warren, A., 1996. The role of streamline curvature in sand dune dynamics: evidence from field and wind tunnel measurements. Geomorphology 17. http://dx.doi.org/10.1016/0169-555X(95)00093-K.

Further reading

Blasius, H., 1913. Das Aehnlichkeitsgesetz bei Reibungsvorgängen in Flüssigkeiten. Mitt. Forsch.arb. Geb. Ing.wes. 131. http://dx.doi.org/10.1007/978-3-662-02239-9_1.

Tanaka, K.L., et al., 2014. Geologic map of Mars, USGS Scientific Investigations Map 3292, scale 1:20,000,000, pamphlet 43 pp. http://dx.doi.org/10.3133/sim3292.